ELSEVIER

Journal of Hazardous Materials B96 (2003) 171–188

Journal of Hazardous Materials

www.elsevier.com/locate/jhazmat

Model of spills and fires from LNG and oil tankers

J.A. Fay*

Department of Mechanical Engineering, Massachusetts Institute of Technology, Cambridge, MA 02139, USA

Received 30 March 2002; received in revised form 1 April 2002; accepted 3 June 2002

Abstract

A comprehensive model for predicting the dynamics of spills from LNG and oil product tankers is constructed from fluid mechanics principles and empirical properties of oil and LNG spills on water. The analysis utilizes the significant tanker hold and discharge flow area dimensions to specify the cargo liquid outflow history and the ensuing pool characteristics, including the establishment of a pool fire. The pool fire area, duration, and heat release rate are determined as functions of the tanker cargo variables. Examples of an LNG and gasoline spill show that for likely discharge flow areas these spills may be regarded as instantaneous, simplifying the evaluation of risk consequences.
© 2002 Elsevier Science B.V. All rights reserved.

Keywords: LNG; Pool fire; Tanker spills; Oil products; Spill model; Underwater spill

1. Introduction

The great increase in oceanic shipping of crude oil in large supertankers following World War II, and the subsequent occasional accidental episodes of disastrous oil spills from these vessels that harmed coastal environments, led to development of models for the spread of oil spills on the surface of the sea [1] and corroborating laboratory measurements [2]. These models confirmed the common observation that significant spills spread rapidly to encompass large areas of the ocean surface, well beyond the capacity to contain them by mechanical means within the short time of spreading.

In the 1970s, the development of oceanic tankers transporting cryogenic liquids (LNG, LPG, ethylene) posed additional spill risks of combustion, either at the spill site or at downwind locations to which the spill vapors might travel [3,4]. In the intervening years, a considerable amount of theoretical and experimental research has been conducted on the evaporation of cryogenic spills on land and water, the dispersion and combustion of

* Tel.: +1-617-253-2236; fax: +1-617-258-8559.
E-mail address: jfay@mit.edu (J.A. Fay).

0304-3894/03/$ – see front matter © 2002 Elsevier Science B.V. All rights reserved.
PII: S0304-3894(02)00197-8

the evolved vapor clouds, and the establishment of pool fires at the spill site (for a recent summary, see [5]).

In siting and licensing marine terminals where LNG is landed from tankers, public authorities have had to consider the possibility of accidental spills, usually considered to be a consequence of a ship collision or grounding. But the recent episodes of bombing incidents, including the attack in 2000 on the USS Cole, have raised the issue of other sources of vessel damage that might result in spills that form pool fires alongside the stricken vessel.

Raj and Kalelkar [6] and Raj [7] have considered the formation of an LNG pool fire from a spill of given volume delivered to a level surface (either water or land) at a uniform rate over a given time period. In the limit of very short time, the spill may be considered instantaneous and the resulting pool fire spreads to a size and burns at a rate determined by the spill volume and the LNG fuel properties. In the alternate limit of a long period of spill discharge, the pool fire characteristics are determined by the volumetric discharge rate. In either case, the spill volume and discharge time are exogenous variables determining the pool fire characteristics.

The spill volume, discharge rate, and duration are significant determinants of the spill behavior. For a spill from an ocean tanker, these are dependent upon the tanker hold size and configuration, the size and location of the vessel's rupture opening, and of course, the properties of the cargo fluid. This paper models both the discharge process and the pool spread behavior, expressing the significant results (pool area, pool fire duration, heat release rate) in terms of the tanker hold and rupture variables, covering the entire practical range. Examples are given for spills from typical LNG and oil product tankers.

2. Fluid mechanics of the spill process

Liquid hydrocarbon fuel tankers carry cargo that is less dense than sea water. The requirements for hull strength and reserve buoyancy result in cargo tanks in which the top surface of the liquid cargo is elevated above that of the surrounding sea water, to an extent that creates a liquid hydrostatic pressure within the cargo tank exceeding that of the surrounding atmosphere or sea water at the same elevation. Any puncture of the vessel's side walls permits the cargo to flow out to the surrounding environment at a velocity determined by the pressure difference between the cargo and the exterior atmosphere or sea water at the level of the puncture opening.

The emerging hydrocarbon cargo fluid, being immiscible with and less dense than sea water, floats on the sea water surface. It forms a pool, centered at the rupture site, that spreads horizontally, induced by a horizontal pressure gradient resulting from the gravitational force on the liquid layer. For the very large spill rates being considered here, the spreading rate is governed by a balance between fluid inertia and the gravity force, called gravity–inertia spread [1]. Although the spreading of the pool is enhanced by the flow of liquid from the cargo tank, it nevertheless continues as long as there is a finite volume of liquid in the pool.

The pool fluid can be vaporized by two processes. If it is a cryogenic fluid, such as liquified natural gas, propane, or ethylene, having a boiling point below the sea water temperature, it will boil vigorously by virtue of its contact with the underlying sea water. If vapor evolving from the pool catches fire, establishing a pool fire above the spreading liquid fuel, thermal

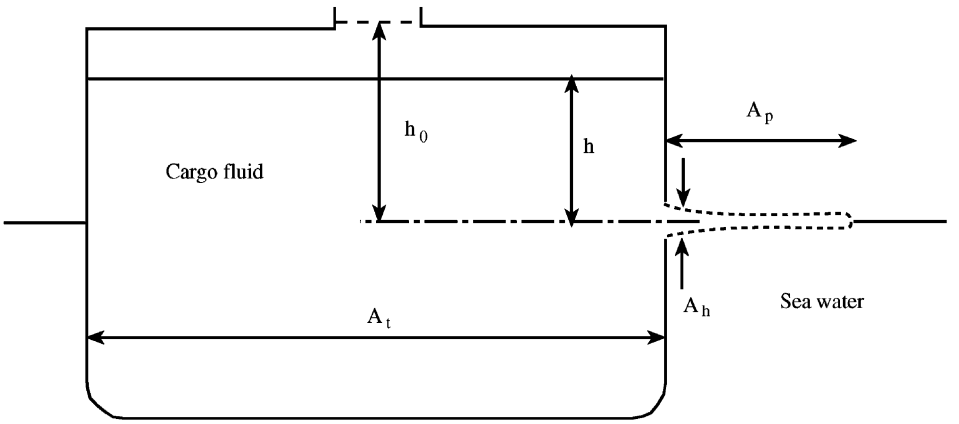

Fig. 1. A sketch of the cross-section of a tanker vessel, showing the configuration of the cargo fluid in a tanker during outflow through a rupture in the side of the vessel.

radiation from the pool fire will heat and vaporize the liquid fuel. In the case of pool fires above cryogenic fuel spills, both processes act in parallel to increase the rate of vaporization.

The configuration of the cargo fluid in a tanker hold during its flow out through a rupture at the level of the waterline is sketched in Fig. 1. The rupture flow area is denoted by A_h, while the upper surface area of the cargo fluid is A_t. The time-varying hydrostatic head h governing the fluid velocity through the rupture is, in this case, the vertical distance from the rupture centerline to the free surface of the cargo fluid. The lateral area of the liquid pool outside the vessel, A_p, is a function of time, depending upon the spreading of the cargo fluid that leaks from the tank.

There is a time scale t_d that characterizes the duration of the outflow from the ruptured cargo tank. The magnitude of the outflow velocity through the rupture is $\sqrt{gh_0}$, so that the outflow volume flow rate $\sqrt{gh_0}A_h$ times the discharge time t_d must equal the volume $A_t h_0$ discharged (where h_0 is the initial value of h), giving

$$t_d \sim \frac{A_t h_0}{\sqrt{gh_0}A_h} = \frac{A_t}{A_h}\sqrt{\frac{h_0}{g}} \tag{1}$$

Whether the liquid pool formed from this discharge is vaporized by boiling or the establishment of a pool fire, it cannot be depleted in a time shorter than t_d.

The rate of loss of the pool liquid by vaporization may be characterized by a regression velocity w, where the volume rate of pool liquid vaporized per unit surface area is w. The regression velocity is a function of the processes that evaporate the fluid, boiling and/or pool fire heating, and the fluid properties. It is this regression velocity which limits the maximum size of the pool area, which would otherwise continue to increase indefinitely [1].

We can distinguish two limiting cases of pool size. If the rupture area A_h is very small, a quasi-steady pool evaporation process will be established, for which the evaporation rate from the pool will equal the discharge rate from the vessel. In this case, the lifetime of the pool formation and extinction will equal the discharge duration t_d. Alternatively, if the

rupture area A_h is very large, the pool will spread as if from an instantaneous discharge and will persist for a much longer time than t_d in order to vaporize all the discharged volume.

The maximum pool area for the case of small A_h may be found by equating the discharge volume flow rate $\sqrt{gh_0}A_h$ to the vaporization rate wA_p, giving

$$A_p \sim \frac{\sqrt{gh_0}A_h}{w} \tag{2}$$

Because w is always quite small compared to $\sqrt{gh_0}$ for practical cases, the pool area is large compared with the rupture area.

Estimating the corresponding evaporation time and pool area for the case of large rupture area is complicated by the dynamics of the pool spreading. For the latter, the pool area A_p resulting from an instantaneous spill of volume $A_t h_0$, after a time t_v, is approximately [1,3]

$$A_p \sim (\sqrt{g\Delta(A_t h_0)})t_v \tag{3}$$

where

$$\Delta \equiv \frac{\rho_w - \rho_f}{\rho_w} \tag{4}$$

ρ_w and ρ_f being the sea water and cargo fluid mass densities, respectively. Setting the evaporation loss from the pool during the time t_v equal to the cargo spill volume,

$$A_p w t_v \sim h_0 A_t \tag{5}$$

we can solve Eqs. (3) and (5) for the evaporation time and pool area at that time:

$$t_v \sim \frac{(A_t h_0)^{1/4}}{w^{1/2}(g\Delta)^{1/4}} \tag{6}$$

$$A_p \sim \frac{(A_t h_0)^{3/4}(g\Delta)^{1/4}}{w^{1/2}} \tag{7}$$

We may now contrast the behavior of the pool formation and ultimate disappearance for small and large A_h. For small A_h, the pool area is a maximum at the beginning of the spill, declining in size in proportion to the outflow rate and disappearing at the discharge duration given in (1). The maximum pool area is proportional to A_h (see (2)), and the pool evaporation time is inversely proportional to A_h (see (1)). In contrast, for very large A_h, the pool size grows during the outflow process, reaching a maximum size at the end of the pool evaporative lifetime (6) as given in Eq. (7). In this case, both the evaporative time and the maximum pool size are independent of the hole size A_h, provided it is large enough. But both the small and large A_h approximations give equal values for A_p and t_v when A_h is:

$$A_h \sim A_t^{3/4} w^{1/2} \Delta^{1/4} \left(\frac{h_0}{g}\right)^{1/4} \tag{8}$$

It is this value of A_h that determines whether A_h is small or large. It will be seen below that the ratio of the two sides of (8) is a parameter in an exact description of the pool behavior.

2.1. Analytical model

To develop a more accurate model of the spill and pool behavior, we begin by considering the outflow through the puncture area A_h. Equating the rate of loss of cargo volume to the outflow volumetric flow rate,

$$-\left(\frac{d(hA_t)}{dt}\right) = \sqrt{2gh}A_h \tag{9}$$

we obtain, by integration,

$$h = \begin{cases} \left(\sqrt{h_0} - \sqrt{\frac{g}{2}}\frac{A_h}{A_t}t\right)^2, & \text{if } 0 \le t \le \sqrt{\frac{2h_0}{g}}\left(\frac{A_t}{A_h}\right) \\ 0, & \text{if } t \ge \sqrt{\frac{2h_0}{g}}\left(\frac{A_t}{A_h}\right) \end{cases} \tag{10}$$

We next determine the rate of change of volume V_p of the fluid in the pool, as a consequence of the inflow from the rupture minus the evaporation from the pool area A_p:

$$\frac{dV_p}{dt} = \sqrt{2gh}A_h - wA_p \tag{11}$$

We now express the spreading rate of the pool, which is assumed to be semicircular in shape, of radius R and area $A_p = \pi R^2/2$, in the form given in [3]:

$$\frac{dR}{dt} = \beta\left(g\Delta\frac{V_p}{\pi R^2/2}\right)^{1/2} \tag{12}$$

where β is an empirical constant and the factor $V_p/(\pi R^2/2)$ is the average thickness of the pool. This may be transformed to the form:

$$\frac{dA_p}{dt} = \frac{d(\pi R^2/2)}{dt} = \beta\sqrt{2\pi g\Delta V_p} \tag{13}$$

defining the time rate of growth of the pool area.

Eqs. (10), (11) and (13) define the time history of the outflow from the vessel and the subsequent pool formation and vaporization. As described in Section 2, the nature of this history depends critically on the size of A_h through its relationship to other parameters of the flow. To proceed to elucidate and simplify this relationship, it is useful to express these equations in dimensionless form. To this end we choose the following dimensionless variables:

$$t^* \equiv \left(\frac{A_h}{A_t}\right)\sqrt{\frac{g}{h_0}}t, \qquad v^* \equiv \frac{V_p}{h_0A_t}, \qquad a^* \equiv \frac{wA_p}{A_h\sqrt{gh_0}}, \qquad h^* \equiv \frac{h}{h_0} \tag{14}$$

Here we have introduced time, volume, area, and length scales $(\sqrt{h_0/g}A_t)/A_h$, h_0A_t, $A_h\sqrt{gh_0}/w$, and h_0 to define the dimensionless variables. Eqs. (10), (11) and (13) then

assume the form:

$$h^* = \begin{cases} \left(1 - \dfrac{t^*}{\sqrt{2}}\right)^2, & 0 \le t^* \le \sqrt{2} \\ 0, & t^* \ge \sqrt{2} \end{cases} \tag{15}$$

$$\frac{\mathrm{d}v^*}{\mathrm{d}t^*} = \sqrt{2h^*} - a^* \tag{16}$$

$$\frac{\mathrm{d}a^*}{\mathrm{d}t^*} = \phi\sqrt{v^*} \tag{17}$$

where the parameter ϕ has the value

$$\phi \equiv \beta\sqrt{2\pi\,\Delta w}\sqrt{\frac{h_0}{g}}\frac{A_\mathrm{t}^{3/2}}{A_\mathrm{h}^2} \tag{18}$$

By comparison with (8), we now see that $\phi \gg 1$ corresponds to small A_h while $\phi \ll 1$ defines the case of large A_h.

Before proceeding to discuss the solutions for particular values of ϕ, we develop a general relation for the time-averaged value of a^*, denoted by $\overline{a^*}$. Integrating (15) and (16) over the time interval ($t_\mathrm{v}^* \ge \sqrt{2}$) for the pool to evaporate, we find

$$\overline{a^*} = \frac{1}{t_\mathrm{v}^*} \tag{19}$$

This relationship expresses the conservation of mass; all of the cargo fluid drained from the ship's hold is evaporated from the fluid pool by the end of the evaporation period t_v^*.

2.1.1. $\phi \gg 1$

In this case, after a short period of time $t_\mathrm{s}^* \ll \sqrt{2}$ of unsteady flow, a quasi-steady flow will be established during which the inflow to the pool is balanced by evaporation. This balance is expressed by setting the right side of (16) equal to zero, giving a^* as a function of time:

$$a^* = \sqrt{2} - t^*, \quad t_\mathrm{s}^* \le t^* \le \sqrt{2} \tag{20}$$

During this time, the pool area shrinks linearly with time, reaching zero at the end of the discharge, when $t^* = \sqrt{2}$. The pool area at the beginning of the quasi-steady flow, a_s^*, becomes

$$a_\mathrm{s}^* = \sqrt{2} - t_\mathrm{s}^* \tag{21}$$

We next consider the transient flow time period $0 \le t^* \le t_\mathrm{s}^*$, for which $t^* \ll \sqrt{2}$ and $h^* = 1$. Eq. (16) becomes

$$\frac{\mathrm{d}v^*}{\mathrm{d}t^*} = \sqrt{2} - a^* \tag{22}$$

This may be solved simultaneously with (17) to determine v^* as a function of a^*:

$$v^* = \left[\frac{3a^*}{2\phi}\left(\sqrt{2} - \frac{a^*}{2}\right)\right]^{2/3} \tag{23}$$

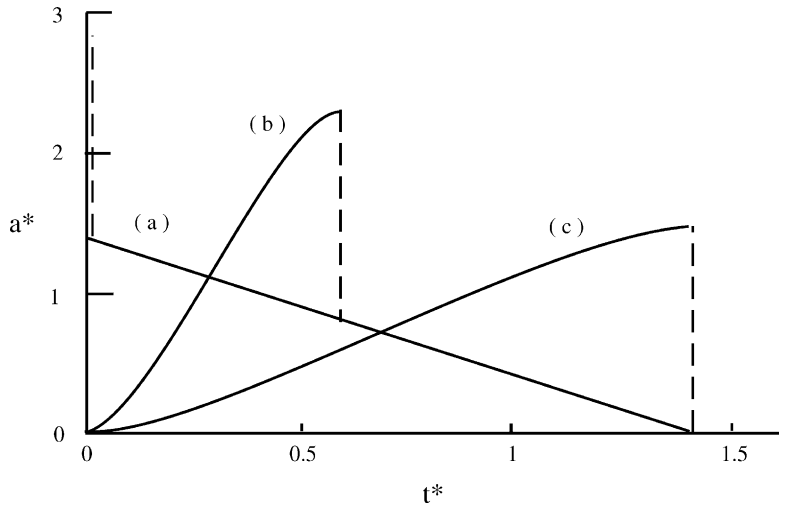

Fig. 2. The dependence of pool area a^* on time t^* for large values of the flow parameter ϕ: (a) $\phi \to \infty$; (b) $\phi = 10$; (c) $\phi = \phi_c = 1.784$.

The pool volume increases during this period, reaching a maximum when $a^* = \sqrt{2}$ and then decreasing to zero when a^* reaches its maximum value, a_m^*, of

$$a_m^* = 2\sqrt{2} \tag{24}$$

Note that $a_m^* \geq \sqrt{2}a_s^*$; the transient phase leaves a larger pool than that at the beginning of the quasi-steady phase. The duration of the transient flow may be found by substituting (23) in (17):

$$t_s^* = \phi^{-2/3} \int_0^{2\sqrt{2}} \frac{\mathrm{d}a^*}{[(3a^*/2)(\sqrt{2} - a^*/2)]^{1/3}}$$
$$= \left(2^{7/6}(3^{2/3})\frac{(\Gamma\{4/3\})^2}{\Gamma\{5/3\}}\right)\phi^{-2/3} = 4.124\phi^{-2/3} \tag{25}$$

where $\Gamma\{x\}$ is the gamma function of argument x.

For $\phi \to \infty$, the transient phase is negligible in duration, and the quasi-steady flow occupies all but the very beginning of the outflow. The dependence of area a^* on time t^* for this case is shown in Fig. 2(a).

In cases where ϕ is not sufficiently large to satisfy the requirement that $t_s^* \ll \sqrt{2}$, Eqs. (15)–(17) must be integrated numerically. An example is shown in Fig. 2(b) for $\phi = 10$. Here the transient phase is extended to $t_s^* = 0.588$, where $a_m^* = 2.233$ and $a_s^* = 0.827$, both lower than the values of $2\sqrt{2}$ and $\sqrt{2}$, respectively for $\phi \to \infty$. Note that a^* varies approximately linearly with t^* in the transient phase, and exactly so in the quasi-steady phase.

For even lower values of ϕ, the transient phase time t_s^* increases while a_m^* and a_s^* decrease, until at a critical value of $\phi_c = 1.784$, $t_s^* = \sqrt{2}$ and the transient phase occupies the whole of the outflow duration. For this example, shown in Fig. 2(c), $a_m^* = 1.431$ at $t_v^* = \sqrt{2}$.

2.1.2. $\phi \ll 1$

In this limit, the discharge occurs quickly, then the pool spreads and evaporates. Focusing first on the short discharge period where $0 \le t^* \le \sqrt{2}$, we may neglect the evaporation term in (16) and find by integration the time dependence of v^*:

$$v^* = \sqrt{2}t^*\left(1 - \frac{t^*}{2\sqrt{2}}\right), \quad t^* \le \sqrt{2} \tag{26}$$

Combining this with (17) and integrating over the discharge period, we find the pool area a_d^* at $t^* = \sqrt{2}$ to be

$$a_d^* = 2^{1/4}\phi \int_0^{\sqrt{2}} \left(t^*\left[1 - \frac{t^*}{2\sqrt{2}}\right]\right)^{1/2} \mathrm{d}t^* = \frac{\pi}{2\sqrt{2}}\,\phi \tag{27}$$

For subsequent times where $t^* \ge \sqrt{2}$, Eqs. (16) and (17) then have the form

$$\frac{\mathrm{d}v^*}{\mathrm{d}t^*} = -a^* \tag{28}$$

$$\frac{\mathrm{d}a^*}{\mathrm{d}t^*} = \phi\sqrt{v^*} \tag{29}$$

with the initial conditions at $t^* = \sqrt{2}$ that $v^* = 1$ and $a^* = a_d^*$, as determined above. Integrating, we find the variation of v^* with a^*:

$$v^* = \left(1 - \frac{3}{4\phi}[(a^*)^2 - (a_d^*)^2]\right)^{2/3} \tag{30}$$

The maximum pool area a_m^* occurs when $v^* = 0$:

$$(a_m^*)^2 = \frac{4\phi}{3} + \left(\frac{\pi\,\phi}{2\sqrt{2}}\right)^2$$

$$a_m^* \simeq \left(\frac{4\phi}{3}\right)^{1/2}\left[1 + \frac{3\pi^2}{64}\phi\right] = 0.971\,\phi^{1/2}(1 + 0.463\phi) \tag{31}$$

The time t_v^* required to evaporate the pool may be found by combining (31) with (29) and integrating,

$$\int_{\sqrt{2}}^{t_v^*} \mathrm{d}t^* = \frac{1}{\phi}\int_{a_d^*}^{a_m^*} \frac{\mathrm{d}a^*}{\sqrt{v^*}}$$

$$t_v^* = \frac{\sqrt{3\pi}}{2}\frac{\Gamma\{5/3\}}{\Gamma\{7/6\}}\phi^{-1/2} + \sqrt{2} - \frac{\pi}{2\sqrt{2}} = 1.493\phi^{-1/2} + 0.304 \tag{32}$$

To find a^* as a function of time, one must integrate (28) and (29). For the limit of $\phi \to 0$, this integration is shown in Fig. 3(a), using modified coordinates of $a^*/\sqrt{\phi}$ versus $t^*\sqrt{\phi}$. As expected, the pool area increases with time until evaporation ceases at $t^*\sqrt{\phi} = 1.493$ where $a^*/\sqrt{\phi} = 1.155$ (see Eqs. (31) and (32)).

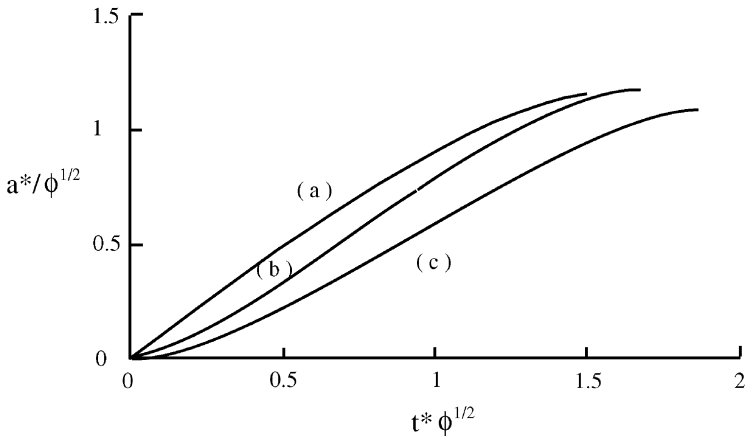

Fig. 3. The dependence of modified pool area $a^*/\sqrt{\phi}$ on modified time $t^*\sqrt{\phi}$ for $\phi \leq \phi_c$: (a) $\phi \to 0$; (b) $\phi = 1/3$; (c) $\phi = \phi_c = 1.784$.

2.1.3. $\phi \leq \phi_c$

In general, for values of ϕ in the range $\phi \leq \phi_c$ that are not small enough that the approximations given above are valid, one must resort to numerical integration of Eqs. (15)–(17) to find the time dependencies of v^* and a^* on t^* and the values of a_m^* and t_v^*. This has been done for the intermediate case of $\phi = 1/3$ and the limiting value of ϕ_c, and are shown in Fig. 3(b) and (c), using modified coordinates.

2.1.4. Summary

The results of the analyses in Sections 2.1.1–2.1.3 above are summarized in Table 1, which lists the values of a_m^*, t_s^*, a_s^*, t_v^*, and $a_m^* t_v^*$, for eight values of ϕ in the range $0 < \phi < \infty$. Considered as functions of ϕ, a_m^* increases, while t_v^* decreases, over the range $0 < \phi < \infty$, reaching the limits of $2\sqrt{2}$ and $\sqrt{2}$, respectively, at $\phi \to \infty$. Their product, $a_m^* t_v^*$, varies little over this entire range, reflecting the fact that $\overline{a^*} t_v^* = 1$ is independent of ϕ (see (19)). We note that the ratio $a_m^*/\overline{a^*}$ lies in the range of 1.724–4.

The data of Table 1 for a_m^* and t_v^* as functions of ϕ are plotted in Figs. 4 and 5, respectively, using logarithmic coordinates. The analytical expressions for $\phi \ll 1$ and $\phi \gg 1$ are shown

Table 1
Pool area and evaporation time

	ϕ							
	$\ll 1$	1/3	1	1.784	3	10	30	$\gg 1$
a_m^*	$1.155\sqrt{\phi}(1 + 0.463\phi)$	0.661	1.113	1.431	1.716	2.233	2.521	2.828
t_s^*				1.414	1.113	0.588	0.300	$4.124\phi^{-2/3}$
a_s^*				0	0.302	0.827	1.114	$(1.414–4.124)\phi^{-2/3}$
t_v^*	$1.493/(\sqrt{\phi} + 0.304)$	2.875	1.775	1.414	1.414	1.414	1.414	1.414
$a_m^* t_v^*$	$1.724 + 0.351\sqrt{\phi}$	1.899	1.976	2.024	2.427	3.157	3.565	4.000

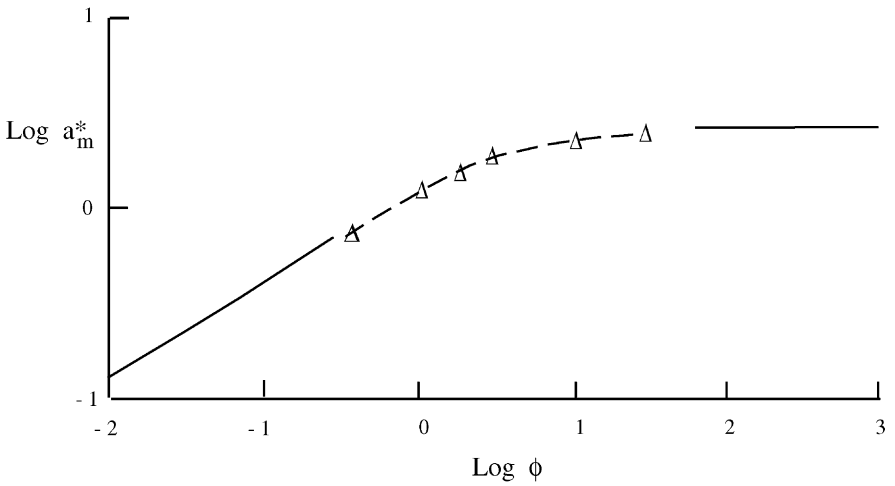

Fig. 4. A plot of the variation of dimensionless maximum pool area a^*_m as a function of the relative outflow parameter ϕ. Data is taken from Table 1.

as solid lines while the numerical values are represented by the symbol △. These latter are connected by a faired dashed line. While the transition from one limit to the other occupies a 100-fold increase in ϕ, this translates into a 10-fold increase in A_h.

Values of small A_h (large ϕ) define the region where quasi-steady flow occurs, but in which there exists some unsteady pool formation. Elsewhere, the pool formation is entirely unsteady.

As mentioned in Section 1, Raj and Kalelkar [6] (see also [8]), have provided solutions that are equivalent to the two limiting cases of Table 1, $\phi \ll 1$ and $\phi \gg 1$. Expressed in terms of the a^* and t^* dimensionless variables, their values for $\phi \gg 1$ are identical to those of a^*_s and t^*_s in Table 1. But for the case of $\phi \ll 1$, they find $a^*_m = 1.56\phi^{1/2}$, $t^*_v = 1.355\phi^{-1/2}$, $a^*_m t^*_v = 2.118$, and $\overline{a}t^*_v = 1$. The first two of these are 35% higher and

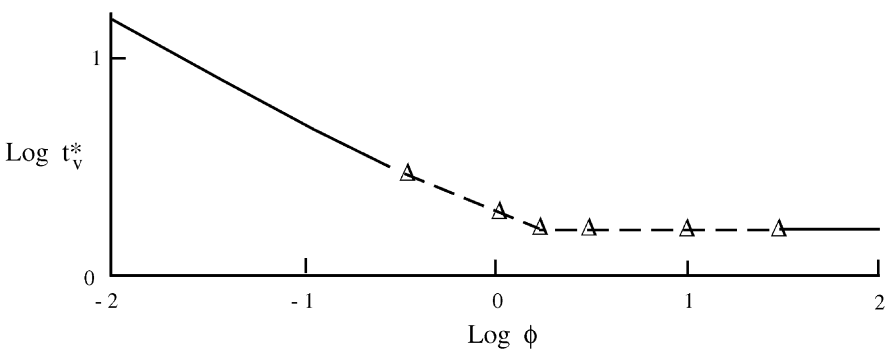

Fig. 5. A plot of the variation of dimensionless evaporation time t^*_v as a function of the relative outflow parameter ϕ. Data is taken from Table 1.

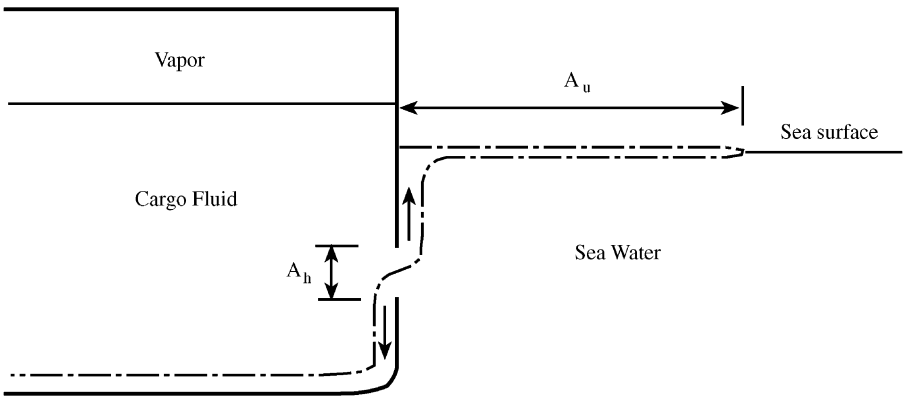

Fig. 6. A sketch of the cargo fluid outflow and sea water inflow through an underwater puncture. The dash-dot line denotes the interface between the cargo fluid and sea water.

10% lower, respectively, than the exact solutions of Table 1. The product $a_{\mathrm{m}}^{*}t_{\mathrm{v}}^{*}$ is 27% higher than the exact value of Table 1 but $\overline{a}t_{\mathrm{v}}^{*}$ is equal to the exact value of (19).

2.2. Underwater punctures

For an underwater puncture, such as might happen in a ship collision or grounding, the effective head h driving the cargo discharge is reduced from that shown in Fig. 1 by an amount $[\Delta/(1-\Delta)]d$, where d is the distance from the waterline to the centerline of the hole in the hull. The initial outflow is that given in Section 2, with h replaced by $\hat{h}$:

$$\hat{h} \equiv h - \left(\frac{\Delta}{1-\Delta}\right) d \tag{33}$$

The initial outflow will cease when $\hat{h} = 0$, with the cargo gas/liquid interface at a distance $[\Delta/(1-\Delta)]d$ above the water line.

At the end of this outflow stage there is, on average, a balance in the hydrostatic pressure between the cargo fluid and the sea water external to the ship, at least at the midlevel of the puncture area. But above and below this level there is an imbalance, such that cargo fluid flows out and sea water flows in, at equal volume flow rates, as illustrated in Fig. 6. The sea water inflow displaces cargo fluid at the bottom of the cargo tank, leading to further discharge of the cargo fluid from below, rather than from above, as in the earlier discharge phase. This discharge continues until the lower part of the cargo hold is filled with sea water, up to the level of the top of the puncture. The less dense cargo fluid is decanted from the hold as sea water intrudes.

The volume flow rate of this discharge may be estimated. Consider first the outflow of the cargo fluid through the upper portion of the puncture. Assuming that the vertical height of the puncture is $\sqrt{A_{\mathrm{h}}}$, and that a fraction f of that height and flow area is occupied by the outflow, the pressure difference driving the outflow is $\sim(\rho_{\mathrm{w}} - \rho_{\mathrm{c}})gf\sqrt{A_{\mathrm{h}}}$ and the

corresponding velocity[1] is $\sim(2[\rho_w - \rho_c]gf\sqrt{A_h}/\rho_c)^{1/2}$, leading to a volume outflow rate dV/dt of

$$\frac{dV}{dt} \sim \left(\frac{2(\rho_w - \rho_c)gf\sqrt{A_h}}{\rho_c}\right)^{1/2} fA_h \sim \left(\frac{2(\rho_w - \rho_c)g(1-f)\sqrt{A_h}}{\rho_w}\right)^{1/2} (1-f)A_h \tag{34}$$

where the term on the extreme right is the equal inflow rate of the sea water. Eliminating f, we find

$$\frac{dV}{dt} = \gamma(2g\Delta_u A_h^{5/2})^{1/2} \tag{35}$$

where γ is an empirical constant of order unity and

$$\Delta_u \equiv \frac{\rho_w - \rho_c}{(\rho_w^{1/3} + \rho_c^{1/3})^3} \tag{36}$$

This outflow is steady during the period of discharge because the driving pressure difference is time invariant. Consequently, after an initial transient flow as in Section 2.1.1, the pool of evaporating cargo fluid formed at the sea surface from the rising column of cargo effluent has a time-invariant area A_u given by

$$A_u = \frac{\gamma(2g\Delta_u A_h^{5/2})^{1/2}}{w} \tag{37}$$

Nevertheless, at large enough A_u, the pool formation will become unsteady, like that for an instantaneous spill.

Any puncture whose vertical extent lies both above and below the vessel's waterline will completely drain the cargo fluid from the hold.

3. Examples

In this section, we consider several examples of calculations for spills from LNG and oil tankers, using typical values of the spill parameters for each type of vessel. The principal parameter variable used to express these examples is the area A_h of the puncture in the side of the vessel, which we assume to lie within the range of 1–100 m^2. The lower value represents the smallest hole of consequence while the higher limit is perhaps the largest to be expected in a severe collision or explosion.

We take as variables of interest the maximum pool area A_m and the vaporization time t_v. Expressed in terms of the dimensionless variables a_m^* and t_v^* and the dimensionless parameter ϕ (Eq. (18)), they are

$$A_m = \left(\frac{A_h\sqrt{gh_0}}{w}\right) a_m^* = \left(\frac{\beta^2(2\pi\Delta)gh_0^3A_t^3}{w^2}\right)^{1/4} \frac{a_m^*}{\sqrt{\phi}} \tag{38}$$

[1] The interface between the cargo fluid and the sea water in the neighborhood of the puncture is unstable, leading to unsteady flow. The steady flow relations used here approximate the time-averaged flow through the puncture.

$$t_{\rm v} = \left(\frac{A_{\rm t}}{A_{\rm h}}\right)\sqrt{\frac{h_0}{g}}t_{\rm v*} = \left(\frac{A_{\rm t}h_0}{\beta^2(2\pi\,\Delta)gw^2}\right)^{1/4} t_{\rm v}^*\sqrt{\phi} \tag{39}$$

where the dependence upon the parameter $A_{\rm h}$ is expressed through the value of ϕ in (38) and (39) and the implicit dependence of $a_{\rm m}^*$ and $t_{\rm v}^*$ on ϕ (see Table 1 and Figs. 4 and 5).

As explained in Section 2, there is a critical value of $A_{\rm h}$ (Eq. (8)) that distinguishes between the mostly quasi-steady outflow and pool formation from a small puncture and the rapid unsteady outflow from a large hole. We may calculate this critical value $(A_{\rm h})_{\rm c}$ from Eq. (18) by using the value of $\phi_{\rm c} = 1.784$ from Table 1, obtaining

$$(A_{\rm h})_{\rm c} = 0.749\left(\frac{\beta^2(2\pi\,\Delta)w^2h_0A_{\rm t}^3}{g}\right)^{1/4} \tag{40}$$

The corresponding critical values of $A_{\rm m}$ and $t_{\rm v}$ are found from Eqs. (38) and (39) and Table 1 to be

$$(A_{\rm m})_{\rm c} = 1.071\left[\frac{\beta^2(2\pi\,\Delta)gh_0^3A_{\rm t}^3}{w^2}\right]^{1/4} \tag{41}$$

$$(t_{\rm v})_{\rm c} = 1.889\left[\frac{A_{\rm t}h_0}{\beta^2(2\pi\,\Delta)gw^2}\right]^{1/4} \tag{42}$$

In the case of pool fires, thermal radiation can be estimated from the heat release rate of the combustion of the liquid fuel. The heat release rate $Q_{\rm av}$ averaged over the duration of the pool fire is determined from

$$Q_{\rm av} = \frac{(h_0A_{\rm t})\rho_{\rm c}h_{\rm c}}{t_{\rm v}} \tag{43}$$

where $h_{\rm c}$ is the fuel heating value per unit mass. For underwater punctures, the steady flow heat release rate $Q_{\rm u}$ is found from Eq. (37) to be

$$Q_{\rm u} = \frac{\gamma(2g\,\Delta_{\rm u}A_{\rm h}^{5/2})^{1/2}}{w}\rho_{\rm c}h_{\rm c} \tag{44}$$

The thermal radiative flux q at a distance r from the center of the pool fire is sometimes estimated as [8]:

$$q = \frac{\eta Q}{4\pi r^2} \tag{45}$$

where η is the fraction of the pool heat release rate Q that is emitted as thermal radiation. Eq. (45) only applies at large distances from the pool fire.

3.1. LNG tanker pool fire

LNG tankers carry a liquid cargo having a density 42% of that of sea water. The cargo volume exceeds the displacement volume of the fully-loaded vessel by 30–50%, with the

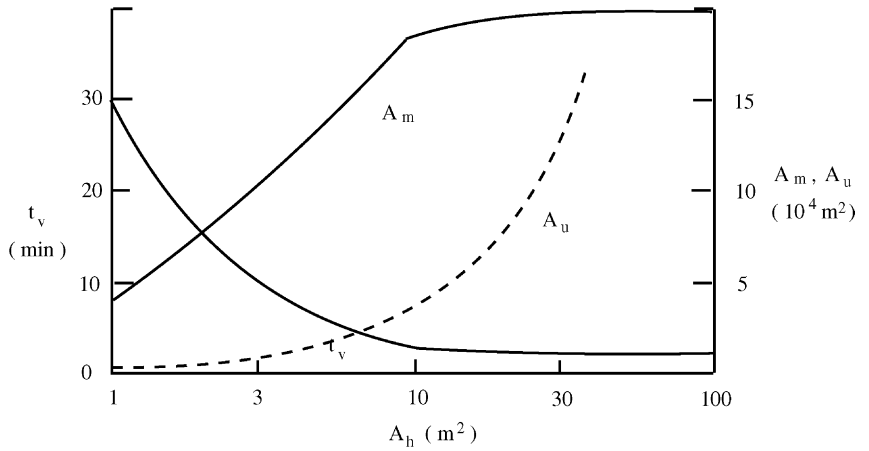

Fig. 7. Solid lines represent the maximum pool area A_m and pool fire duration t_v for a 14,300 m^3 spill from a single hold of an LNG tanker as a function of the puncture area A_h. Dashed line denotes the pool area A_u for an underwater puncture.

result that more than half the cargo volume is elevated above the vessel waterline.[2] If DR is the fully-loaded draft (vertical distance from the waterline to the keel), then for a typical LNG tanker the initial height h_0 of the upper surface of the cargo fluid above the waterline is about 1.1DR. The cargo surface area A_t is related to the cargo tank volume CTV by $A_t \simeq 0.52(\text{CTV/DR})$. For an LNG tanker of 125,000 m^3 cargo capacity, with an 11.8 m draft and 25,000 m^3 cargo tank volume, $h_0 = 13$ m and $A_t = 1100$ m^2. The volume of the spilled fluid, $h_0 A_t$, is 14,300 m^3. These values are used in subsequent calculations.

The LNG pool spreading and evaporation are determined by the parameters Δ, β, and w. For LNG spreading on sea water, $\Delta = 0.58$. In axisymmetric pool spreading, $\beta = 4/\sqrt{3} = 2.31$ [2]. For confined LNG pool fires where heating from the substrate below is inconsequential, $w = 1.9 \times 10^{-4}$ m/s [5]. For confined LNG spills on water, the maximum evaporation rate is $w = (5\text{–}7) \times 10^{-4}$ m/s; it is thought that this rate applies to unconfined spills on water [9]. Assuming that these rates should add for an unconfined pool fire on water, which is simultaneously heated from above by the pool fire and below by the warmer water, we choose $w = 8 \times 10^{-4}$ m/s.

A plot of the maximum pool area A_m and pool fire duration for an LNG tanker spill from a 25,000 m^3 hold, as a function of the puncture area A_h, is shown in Fig. 7. For A_h less than the critical value of 9.09 m^2 (see Eq. (41)), the pool area increases to 18.1×10^4 m^2,[3] while the pool fire duration t_v decreases to 3.3 min, as A_h increases to its critical value. This is the range of mostly quasi-steady flow, where the pool fire tends to consume the LNG as fast as it is disgorged onto the sea surface. For A_h greater than the critical value, there is little change in the values of A_m and t_v within the 10-fold increase in A_h shown in Fig. 7.

[2] Cryogenic liquid cargoes are carried in separate inner thermally insulated tanks that are supported by the ship's structure, in contrast with oil tankers where the cargo tank and ship structure are identical.

[3] The maximum radius of this semicircular pool is 339 m, greater than the length of about 270 m of the LNG tanker being considered.

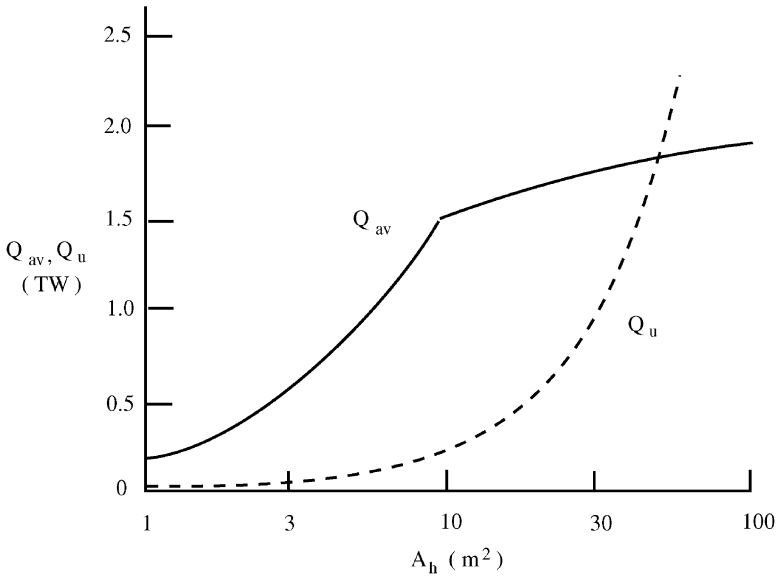

Fig. 8. Solid line represents the time-averaged heat release rate Q_{av} of a pool fire formed from a 14,300 m^3 spill from a single hold of an LNG tanker as a function of the puncture area A_h. Dashed line represents the heat release rate Q_u for an underwater puncture.

The pool fire area A_u for an underwater puncture of area A_h is shown in Fig. 7 as a dashed line. These values are computed from Eq. (37), which assumes a balance between outflow (which is steady) and vaporization. But for the highest values of A_u shown, the high discharge rates imply a transition to unsteady pool growth and a limiting pool area as in the case of above-water discharges. The corresponding pool areas for such conditions have not been calculated.

The time-averaged heat release rate Q_{av} from a pool fire for this spill is plotted in Fig. 8, as a function of the puncture area A_h. Its value at the critical condition is 1.53 TW. As was the case for the other variables shown in Fig. 7, Q_{av} shows less variability for supercritical values of A_h than for subcritical ones.

Also plotted as a dashed line in Fig. 8 is the heat release rate Q_u for an underwater release. The limiting value for large release rates is not shown. Compared to above-water punctures, underwater ones provide smaller values of pool area and heat release rate, for a given A_h, but nevertheless reach the above-water values at large enough A_h.

The distance r to a thermal radiation flux of $q = 5\,kW/m^2$, a criterion of human safety [8], may be calculated from Eq. (45) to be 1.9 km for the critical Q_{av} of an above-water release, if one assumes the lowest empirical value of $\eta = 0.15$ [8].

3.2. Oil tanker pool fire

In contrast to LNG tankers, oil product tankers have less freeboard compared with their draft, a consequence of the higher density of oil products. Also, their cargo holds are

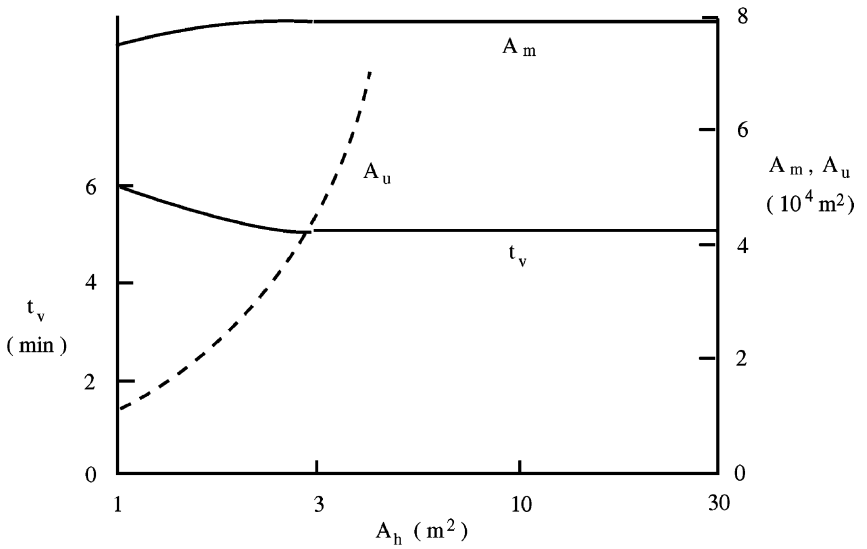

Fig. 9. Solid line denotes the maximum pool area A_m and pool fire duration t_v for a 1140 m^3 spill of gasoline from a wing and centerline hold of an oil tanker as a function of the puncture area A_h. Dashed line denotes the pool area A_u for an underwater puncture.

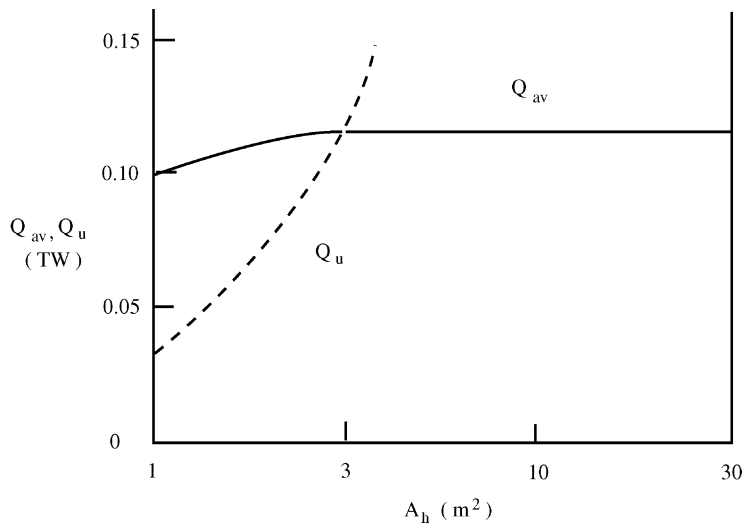

Fig. 10. Solid line denotes the time-averaged heat release rate Q_{av} of a pool fire formed from a 1140 m^3 spill of gasoline from a wing and centerline hold of an oil tanker as a function of the puncture area A_h. Dashed line represents the heat release rate Q_u for an underwater puncture.

subdivided by longitudinal bulkheads into port, starboard, and centerline compartments. For this example, we choose a 41,000 deadweight tonne oil tanker [10] having a combined wing and center tank surface area $A_t = 285\,m^2$ and $h_0 = 4\,m$. The spill volume, $h_0 A_t = 1140\,m^3$, is only a quarter of the hold volume of $4450\,m^3$. We assume a cargo of gasoline, with density $\rho_c = 720\,kg/m^3$ and fuel heating value $h_c = 43.6\,MJ/kg$. For a gasoline pool fire, we choose an evaporation rate of $w = 0.8 \times 10^{-4}\,m/s$ [8].

The maximum pool area A_m and pool fire duration t_v for a $1140\,m^3$ spill of gasoline from a wing and centerline hold of an oil tanker is plotted in Fig. 9 as a function of the puncture area A_h. For puncture areas greater than a few square meters, the discharge time is short enough that the spill may be considered instantaneous, with a maximum area of $79{,}700\,m^2$ and a burnup time of 5.1 min. Compared with the Section 3.1 LNG spill of more than 10 times this volume, the maximum pool area is about one-third as great and the fire duration is 50% longer. These differences are primarily a consequence of the spill volume and regression rate w. Also shown in Fig. 9 is the pool area A_u resulting from an underwater puncture, for the limited hole size where a steady discharge is maintained.

As was done for the LNG spill of Section 3.1, we plot in Fig. 10 the time-averaged heat release rate Q_{av} as a function of the puncture area A_h. For large enough A_h, Q_{av} is 0.116 TW, only about 8% of that for the LNG spill example. This difference reflects the smaller spill volume and longer fire duration. Also shown in Fig. 10 is the heat release rate Q_u for an underwater puncture.

4. Conclusions

When the cargo hold of a tanker is ruptured, the fluid cargo flows out of the hold onto the surface of the ocean, in an amount and at a rate that depends upon the size and location of the rupture and the dimensions and vertical placement of the hold with respect to the sea surface. The outflow volume is ultimately limited by the establishment of a static equilibrium between the fluid remaining in the hold and the external sea water, while the rate of outflow can be estimated from inviscid gravity flow relations. The spilled fluid spreads on the sea surface, eventually evaporating entirely by heating from below (in the case of cryogenic fluids) and/or above if a fire is established above the pool. This dynamic outflow and pool development is a time-dependent process.

A model of the outflow and pool development processes, expressed in dimensionless form, is shown to be dependent upon a single parameter (ϕ, Eq. (18)) whose value distinguishes the extreme cases of a relatively small puncture area having a slow discharge rate from its inverse. In the former case, the pool fire characteristics are determined by the discharge rate; in the latter case, the spill volume is determinative.

For cargo hold punctures that are completely or partially below the sea surface, additional outflow will ensue, accompanied by sea water intrusion into the cargo hold, at rates that are not yet well determined.

Specific examples of an LNG and oil tanker (gasoline cargo) spills show that the range of credible rupture areas considered ensures that, for all but the smaller areas, the spills can be considered to be instantaneous (and thereby dependent only upon the spill volume). Typical LNG spills are larger in volume (14,000 versus $1100\,m^3$), their pool fires are larger

in area (20 versus 8×10^4 m^2) and greater in combustion heat rate (1.9 versus 0.12 TW), and burn faster (3.3 versus 5.1 min) than oil product spills.

An upper limit to the maximum pool area and a lower limit to the pool fire duration may be obtained from Eqs. (38) and (39) specialized for the case of instantaneous spills ($\phi \to 0$). Using the appropriate values from Table 1 and selecting $\beta = 2.31$ as explained in Section 3.1, these limits become

$$A_\mathrm{m} \leq 2.58 \left(\frac{\Delta g (h_0 A_\mathrm{t})^3}{w^2} \right)^{1/4} \tag{46}$$

$$t_\mathrm{v} \geq 0.785 \left(\frac{A_\mathrm{t} h_0}{\Delta g w^2} \right)^{1/4} \tag{47}$$

where $(h_0 A_\mathrm{t})$ is the volume of the spill and A_m is the maximum area of the semicircular pool.

References

[1] J.A. Fay, in: D. Hoult (Ed.), Oil on the Sea, Plenum Press, New York, 1965, pp. 53–63.
[2] J.A. Fay, in: Proceedings of the Joint Conference on Prevention and Control of Oil Spills, American Petroleum Institute, Washington, DC, 1971, pp. 463–466.
[3] J.A. Fay, Comb. Sci. Tech. 7 (1973) 47–49.
[4] J.A. Fay, Ann. Rev. Energy 5 (1980) 89–105.
[5] F.P. Lees, Loss Prevention in the Process Industries, 2nd Edition, Butterworth–Heinemann, Oxford, 1996, Vol. 1, pp. 15/1–333, Vol. 2, pp. 16/203–204.
[6] P.K. Raj, A.S. Kalelkar, Assessment Models in Support of the Hazard Assessment Book (CG-446-3), US Coast Guard, Washington, DC, 1974.
[7] P.K. Raj, Comb. Sci. Technol. 19 (1979) 251–254.
[8] K.S. Mudan, Prog. Energy Combust. Sci. 10 (1984) 59–80.
[9] National Materials Advisory Board, Safety Aspects of Liquified Natural Gas in the Marine Environment, Pub. NMAB 354, National Academy of Sciences, Washington, DC, 1980.
[10] G.A.B. King, Tanker Practice, Stanford Maritime Ltd., London, 1971.